IPTC-18533-MS

Fracture Characterization by Integrating Seismic-Derived Attributes including Anisotropy and Diffraction Imaging with Borehole Fracture Data in an Offshore Carbonate Field, United Arab Emirates

Enru Liu, Mary Johns, Gregg Zelewski, William A. Burnett, Xianyun Wu, and Jie Zhang, ExxonMobil Upstream Research Co; Joe Molyneux, Formerly ExxonMobil Upstream Research Co. and now in ExxonMobil Canada East; Gene Skeith, Tomohiro Obara, Raed El-Awawdeh, Akmal Sultan, and Abdulrahman Al Messabi, Zakum Development Co

This paper was prepared for presentation at the International Petroleum Technology Conference held in Doha, Qatar, 6–9 December 2015.

Abstract

In this paper, we present a case study of fracture characterization by integrating borehole data with a variety of seismic attributes in a carbonate reservoir from a giant offshore field, United Arab Emirates. The objectives are to determine to what extent seismic data may be confidently used for mapping spatial distributions of subtle faults and fracture corridors in the reservoirs and to better understand the distribution of overburden anomalies (karsts, high impedance channels) for field development planning. Borehole data used in our study include information from core descriptions (fracture density and orientations), image logs, cross-dipole shear-wave anisotropy analysis, and dynamic data (well testing, PLT, tracer, and mud-loss). The seismic attributes include standard and advanced post-stack geometrical attributes; pre-stack seismic azimuthal AVO attributes, and recently developed pre-stack diffraction imaging. We find that there are common features that can be identified in different attributes, and the differences may indicate different scales of fractures. We also observe a qualitative correlation in the area of history match challenges and high anisotropy magnitude, where seismic anisotropy can identify relatively high fracture intensity regions/zones instead of pinpointing individual fractures and complements other attributes as differences do exist between seismically identified fracture zones and well data due to overburden anisotropy, resolution and sampling issues (which are addressed using the synthetic modeling approach). Diffraction attributes have revealed more detailed geological features in overburden (e.g. karsts) and reservoirs (e.g. lineaments) than in reflection data and a comparison with mud loss data in the shallow zones looks promising with a good correlation between mud loss and collapsed features. This work has provided an improved understanding of the applicability of the using multi-seismic attributes for fracture characterizations in carbonate reservoirs.

Introduction

Geophysics plays a unique role in the characterization of natural fractures in carbonate reservoirs, and this is often done through the interpretation of seismic-derived attributes that can be interpreted as indicators of the presence of natural fractures. The most often used attributes are geometrical attributes (e.g. curvatures, dips, and azimuth) and seismic anisotropy (e.g. azimuthal AVO analysis). Recently, diffraction imaging has been developed as alternative (and complementary) technology for fracture and fault identifications. Diffraction imaging is the process of separately imaging diffraction events from a given dataset, and the result of this process is an image (or attribute) which highlights lateral impedance discontinuities in the subsurface, such as those at faults, pinch-outs, karst caverns, etc. At well locations, we sometimes have the luxury of having enough measurements to characterize the zones of interest using cores, FMI, log data as well as dynamic data (e.g. well testing, PLT). We do not normally have enough measurements away from wells. On the other hand, seismic measurements typically provide *indirect* estimates of natural fractures, and therefore in order to have a better description of natural fractures and to understand the impact of fractures on subsurface fluid flow for well planning and field development, it is desirable to integrate borehole fracture data and seismic data.

In this paper, we present a case study of fracture characterization by integrating borehole data with a variety of seismic attributes in a giant carbonate oilfield located in the offshore of Abu Dhabi (Edwards et al., 2006; El-Awawdeh et al., 2008; Zhang et al., 2010; Sultan et al., 2011). The region contains predominantly carbonate sediments that were folded during the Neogene tectonic phase. The field has very gently dipping flanks (1–3º) and is elongated along EW anticlinal axis with extensional and strike-slip fault systems developed across the region. Many low impedance Tertiary and Mid-Cretaceous karsts and Upper Cretaceous high impedance channel deposits have been observed in the overburden formations (Figure 1). The overburden anomalies and hard seafloor are the major sources of seismic noise and pose major challenges to processing and interpretation of seismic data. The reservoir zones are porous, shallow-water, shelf-ramp, grain-dominated carbonate deposits, interbedded with low porosity deeper water argillaceous/carbonates mud-rich dense limestone of the Lower Cretaceous age. The average reservoir porosity varies from 10% to 25% with permeability of 10–100md. The total thickness of the zone of interest is approximately 300m with the thickest reservoir being 50m (Figure 2). In 2001, 1500 km^2 of wide-angle 2C (hydrophone and geophone) OBC data were acquired covering the whole field. The data were processed in 2002 and 2006, and reprocessed in 2009 with the aim to better image the field and mitigate multiples and noise (Reilly et al., 2009). Good quality seismic data is critical for quantitative analysis and for using the data for development well design, and production observation analysis. In our previous study (Liu et al., 2011), we focused on a subset of 3D prestack data ($6.5 \times 9 km^2$), and concluded that the reprocessed data are of sufficient quality for fracture characterization using the technology based on azimuthal anisotropy.

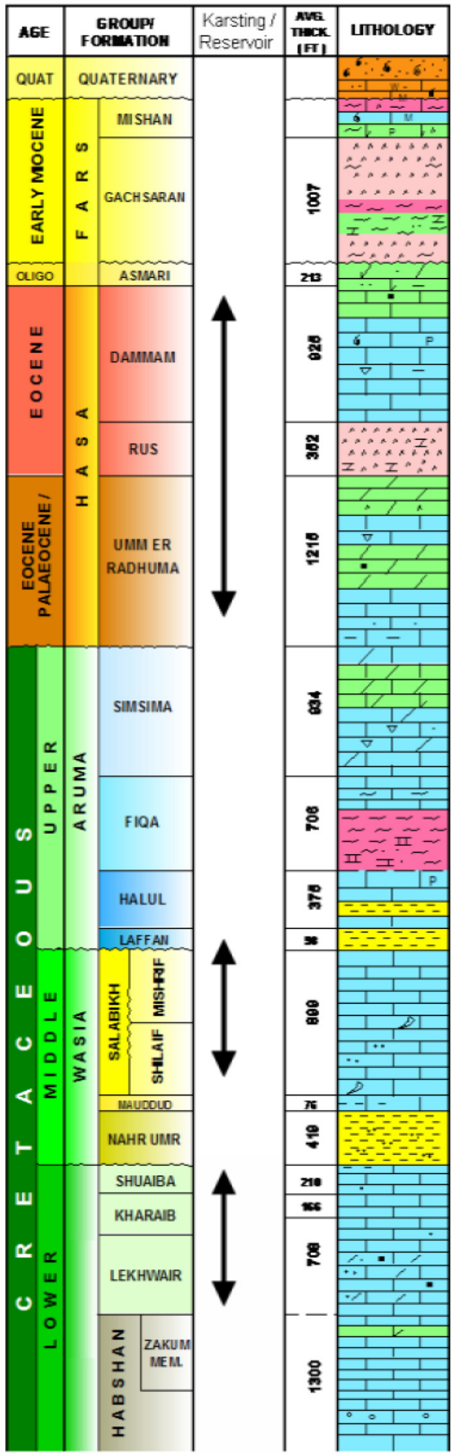

Figure 1—Stratigraphic column showing overburden and reservoir intervals. The top arrows marked the zones where karst and collapsed features are expected, the middle arrow marks the zone where high-velocity channels were interpreted and the lower arrow indicates the reservoir zones (El-Awawdeh et al., 2008; Sultan et al., 2011).

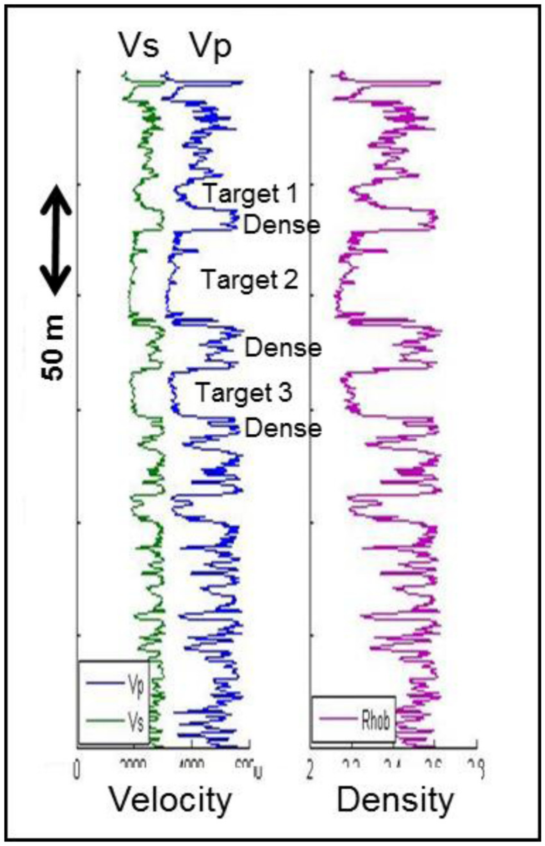

Figure 2—The target reservoirs consist of alternating tight dense and porous carbonate layers. The three main reservoir layers are identified as Targets 1, 2, and 3, each being further subdivided into smaller intervals (Liu et al., 2011).

Evidence of Fractures and Borehole Data

Evidence for the importance of fractures within the target reservoirs is the early water breakthrough that has been observed in reservoirs. The horizontal layering of fractures within the reservoirs is relatively well understood in the thicker reservoirs based on core description. These fractured layers can be addressed in geological models by increasing permeability within these layers. However, it is not well-understood the role of relatively large vertical fractures which cut multiple lithologies. It has been suggested that these relatively large features could have associated fracture clusters and/or corridors that may have a significant impact on fluid flow and overall sweep. Based on outcrop analogs, these features could be tens to hundreds of meters in length and could extend vertically for tens of meters and possibly connect between some reservoirs. Figure 3 shows a conceptual fracture and fault model (Math Williams, per. comm.). In generally, there are four groups of faults and fractures applicable to the study area:

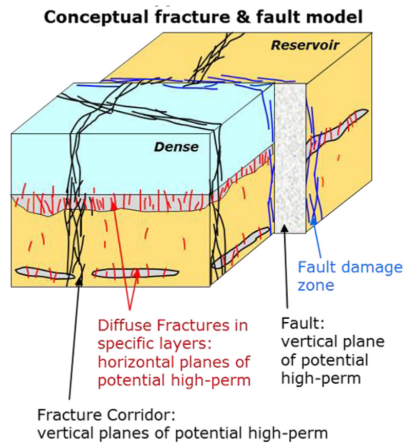

Figure 3—Conceptual fracture models (Math Williams, pers. comm.)

- **Faults**: Faults are fractures along which there have been shearing displacements. They can have various orientations depending on their tectonic style but bedding has less influence on their orientations than it does for joints. Faults can enhance the flow or fluids through rock, or they can act as barriers to fluid flow, depending on their openness and the composition and texture of materials within the fault zone. Three fault sets (defined by strike orientation) have been identified in the field with main fault set (N124°E) aligned along two linear trends: N102°E and N133°E.
- **Diffuse fractures**: These are extensional fractures or joints without shear that are confined to layers parallel to bedding planes, and they do not cut across different lithologies. They include mineralized/cemented veins and tension gashes, although most are non-cemented. In the study area, most of these were formed during diagenesis and are intimately associated with stylolites and other competency contrasts within the limestone. There is a clear correlation between stratigraphy and vertical distribution of these fractures, i.e. some reservoir layers and dense intervals are much more fractured than others.
- **Fracture corridors:** These are thought to be highly fractured zones with about three to ten or more fractures per meter and are often associated with fault zones. Fracture corridors are envisaged to be vertical, high-permeability clusters of fractures that extend from reservoir top to base and can traverse across different reservoirs. They can be heterogeneously distributed both vertically and areally with a large lateral extension from hundreds of meters to several kilometers.
- **Induced fractures**: These are produced during drilling when the mud pressure exceeds the tensile strength of the rock. They may also be caused by a temperature difference between the drilling mud (or injected water) and the formation. Thermally-induced hydraulic fractures form within a few days in the reservoirs as a result of a temperature contrast of 50°C; these are clearly visible on BHI logs such as FMI. In vertical or steeply inclined wells in the reservoir formation the induced fractures form at a strike direction parallel to the maximum horizontal stress, i.e. NNE-SSW, but may range through NS to NNW-SSE.

Large faults with clear displacements can be interpreted from seismic data, and diffuse fractures are likely to be seen in core data. However, there is no direct measure of fracture corridors, and their location, spacing, orientation, length and conductivity are largely unknown, but parameters are required for modeling since they are potentially vertical permeability pathways to shortcut water from injectors to producers, leading to early water breakthrough; and result in poor sweep.

There are abundant wellbore fracture data in the field collected over many years including extensive collection of cores, FMI, cross-dipole data and dynamic data (mud loss, well testing, PLT). Five types of fractures have been identified from core data: larger planar features which cut across the entire the core (F1), fractures nearly cutting across the core (F2), fractures associated with stylolites (F3), discontinuous hairline fractures (F4) and fractures associated with nodules or burrows (F5). The fracture description gives the number of each type of feature, open or closed by core interval, yielding fracture intensity (fractures/ft). Image logs are not used directly in the present study because there are locally strongly influenced by induced fractures, so may be misleading for natural fracture interpretation (Ewart Edwards and Math Williams, pers. comm.). The image logs and interpretations of induced fractures and borehole breakouts, however, are helpful in defining the present day stress direction of N13°E. Several cross dipole data have been acquired, and can be used to provide information about the stress vs fractures through the analysis of dispersion characteristics of fast and slow shear-waves. After separation of fast and slow shear-waves of cross-dipole data, we can compute the dispersion of fast and slow shear waves (i.e. velocity as a function of frequency). If the two dispersion curves are parallel, it is an indication of fracture-induced anisotropy, and if we see a cross-over in the two dispersion curves, they are interpreted as due stress-induced. We have also been supplied with extensive dynamic data in various forms. Basically, there are three kinds of dynamic data: well tests (pressure transient tests), production log tests (PLT's), and mud loss. In this field, the well tests and PLT's are measured at specific point with a reservoir, while mud loss occurs in the shallow zones.

It is normally suggested that all these types of well data are ground-truth for comparison with seismic. It is our understanding that all these well data, to some degree, are detecting different aspects of fractures, but none of them can provide a complete picture of fractures and fracture network, as they are influenced by various environmental factors and need to be interpreted in order to understand their responses to subsurface or near wellbore fractures or fracture distributions.

Figure 4 shows an example of the comparison of shear-wave anisotropy, core fractures, and FMI. We can see a good correlation between shear-wave anisotropy and core open-fracture density. Most open-fractures are seen in relatively thin beds and near the edges of thick beds.

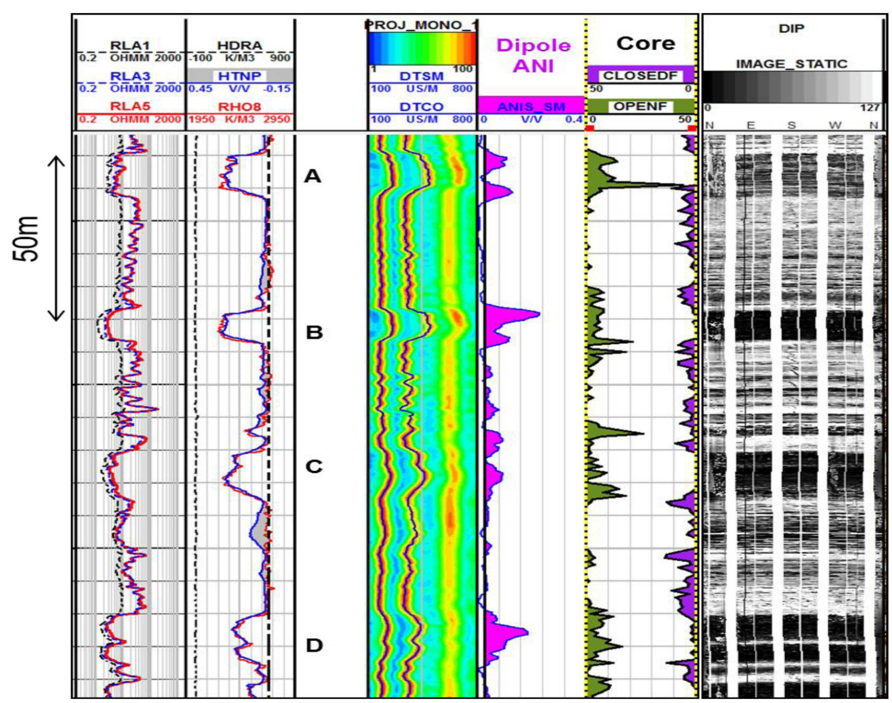

Figure 4—Comparison of dipole shear-wave anisotropy (marked dipole ANI), core fracture, and FMI. There is a good correlation between shear-wave anisotropy and core open-fracture density. Most open-fractures are seen in relatively thin beds and near the edges of thick beds as marked in third target intervals labeled A to D.

Seismic Attributes for Fault and Fracture Identification

The seismic attributes that can be used to characterize fractures can be categorized into three groups: (1) geometrical attributes (e.g. curvatures, dip, azimuth), (2) azimuthal anisotropy (e.g. AzAVO), and (3) newly developed diffraction imaging. Each kind of attributes has its own assumptions and validity and we believe that they are complementary to each other and provide different (sometimes overlapping) information in terms of characterizing subsurface fractures at different scales (Figure 5). It is noted that geometrical and seismic anisotropy attributes which are*indirect* measurements of intermediate-scale features (10^1–10^2m). In contrast, diffraction imaging has gained interest recently as an alternative approach to fracture detection because diffractions are the *direct* seismic wavefield response to intermediate-scale discontinuities. Interpretation of all these seismic attributes (geometrical attributes, anisotropy, diffraction) should be integrated with other data types (e.g., core observations, well logs, borehole washout data, regional stress maps, etc.). Well information can provide excellent overlap of various data types along the borehole axis, but radially, well-log information is both sparse and small-scale (10^{-3}–10^{-1}m). While lateral borehole and seismic scales vastly differ, intermediate-scale borehole-to-surface methods such as VSP or crosswell can help bridge the gap (10^1–10^2m). In the end, it is all about the "*Interpretability*" of various measurements, and no single measurement provides data covering all scales relevant to reservoir description, but having a variety of measurement types can simplify or constrain the geological scaling concepts (Burnett et al., 2015)

	Geological Features	Seismic Observations	Seismic Data Analysis
Macro-scale	Faults	Dislocated Horizons	Geometric Attributes
Meso-scale	Fracture Clusters	Diffractions	Diffraction Imaging
Micro-scale	Diffuse Fractures	Azimuthal time/amplitude variations	Anisotropy Attributes

Figure 5—Different seismic attributes may be used to characterize different scales of fractures and seismic anisotropy is one of the methods used in this work

Geometrical attributes

Geometric attributes, including volumetric estimates of dip and azimuth, curvature, changes in waveform shape, and lateral changes in seismic amplitude, can be used to measure the geometry or shape of seismic reflectors. Coherence is an excellent tool for delineating geological boundaries, and is the most effective and popular method for detecting faults through quantitative estimates of fault/fracture presence. Faults that have drag, are poorly migrated, separate two similar reflectors, or do not appear to be locally discontinuous, will not appear on coherence volumes. These faults do appear in curvature images if there is a change in reflector dip across the fault. Volumetric curvature extends a suite of attributes previously limited to interpreted horizons to the entire un-interpreted cube of seismic data. It is thus relatively more reliable because it is not influenced by subjective judgment of the interpreter. Attributes computation is performed with the goal of deriving or emphasizing those elements of the original seismic data that represent linear geology boundary such as faults. Integration of those lineament characters enhances attribute and amplitude data may become more useful in small fault interpretation. This is particularly true for strike-slip faults with steep surfaces and very small horizontal extent and vertical displacement. The structure oriented filtering (SOF) with edge protection/preservation is often applied to geometrical attributes to smooth the reflectors along its dip in three dimensions between any two neighboring faults/discontinuities while simultaneously sharpening the small faults.

The noise attenuation/mitigation was one of the big efforts in the previous processing and re-processing. In this study, we find that the acquisition footprints and associated linear noise still pose a problem in the attribute computation. Footprint removal is a coherent noise filter that removes acquisition footprint artifacts (e.g. stripping) from input seismic amplitude volumes. The benefits is that the removal of acquisition artifacts early in the workflow provides superior input for follow-on workflow steps by providing high quality resolution of authentic seismic reflections.

Seismic anisotropy

The second kind of attributes that can be used for fracture detection is seismic anisotropy, which refers to the directional variation of velocity and amplitudes with respect to azimuth (Liu and Martinez, 2012). It makes use of the fact that in fractured rock, seismic velocity slows down when the ray path is perpendicular to the fracture orientation, and is less affected when the ray path is parallel to the fracture orientation. As a result, seismic velocity (and therefore) amplitudes are expected to vary as a function of azimuth with respect to the fracture orientation (for simplicity, here we assume one set of vertical fractures). We can either use azimuth velocity-based attributes (low resolution) or azimuth amplitude-based attributes (high resolution) to infer relative anisotropy magnitude (a proxy for fracture intensity) and anisotropy orientation (a proxy for fracture orientation). In our previous study (Liu et al., 2011), azimuthal amplitude variation was used, and we found that the overburden effect was identified as one of the major influencing factors affecting the reliability of fracture interpretation in the targets (Ikawa and Mercado, 2010; Liu et al., 2011). The seismic anisotropy magnitude was computed over intervals for the major reservoirs defined by the seismic interpretation surfaces.

It is noted that other issues such as resolution and detectability of seismic anisotropy and responses of diffuse fractures versus fracture corridors are investigated in the next section using modeling study. Although AzAVO is an attribute associated with an interface or reflector, forward modeling has suggested that because of tuning effects and general seismic resolution of the data, we should not expect to differentiate layers less than about half of the wavelength, i.e. about 50 m. The extraction intervals also visually correlate with the approximate time range of the high anisotropy anomalies. Modeling suggests that anomalies in shallow reservoirs may cause spurious effects on deeper reservoirs. Figure 6 shows a comparison of Targets 1, 2, and 3 reservoir anisotropy with possible stacked anomalies highlighted in red and yellow circles.

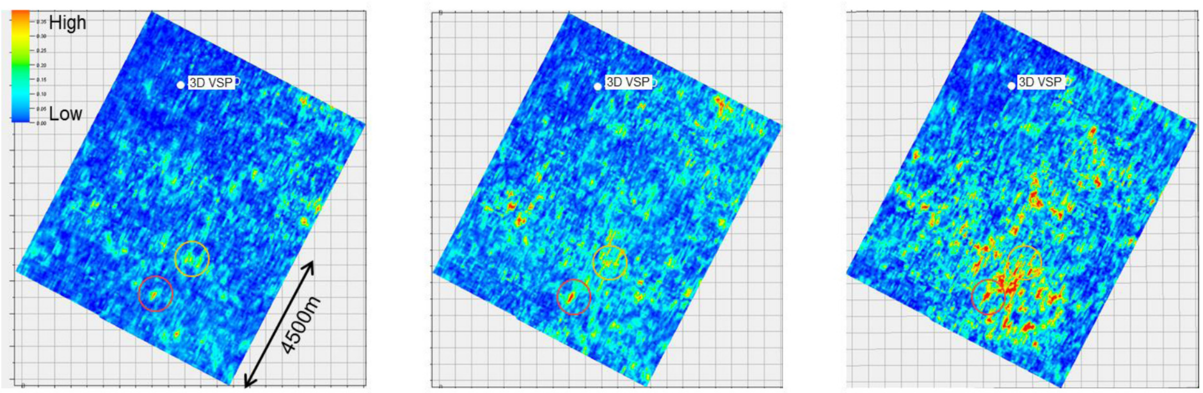

Figure 6—Extracted anisotropy magnitude at three target horizons T1 (left), T2 (middle) and T3 (right) horizons. Circles marked the areas of potential effect of anisotropy in T1 on T2 and T3.

Diffraction imaging

Unlike geometrical attributes and seismic anisotropy, the use of diffraction imaging to detect fractures and other geological features is a relatively new technology (e.g. Guilloux, et al., 2012; Burnett et al., 2015). It is based on the fact that all seismic data contain diffractions, which are the seismic wavefield response to discontinuities and inhomogeneities at all scales. Seismic diffractions, as opposed to specular reflections, occur from subsurface discontinuities such as edges. They can also occur from point features, linear features, or tip features. They have different dynamic (amplitude) characteristics depending on the type of discontinuity, all of which differ from reflection waves (Figure 7). Understanding diffractions can provide information about what types of discontinuities are in the subsurface. Geological examples of real diffraction-generating discontinuities include faults (edge), pinch-outs and rugosity (tip), channels or fractures (linear), or karst features (point or circular shape). Observable diffractions from such features are what seismic diffraction imaging aims to enhance. Many of these geological features diffract the seismic wavefield strongly enough that individual diffraction events are observable in seismic data without any special processing. However, even in the ideal case, a diffraction event at its strongest point has only less than half the amplitude of a reflection with the equivalent impedance contrast. In most cases, diffraction events are typically an order of magnitude weaker than primary reflections. Under conventional processing, diffractions can be attenuated or damaged by reflection-biased processing. Nonetheless, if diffractions are preserved by processing, most modern conventional migration algorithms can handle them accurately. Once they are imaged, diffractions remain weak compared to reflections, to the point that they are rarely interpretable (Figure 8). In order to properly process, image, and interpret the diffracted energy of a seismic wavefield, the diffractions must be separated as early as possible in the processing flow similar to the flow by Zturzu et al. (2015).

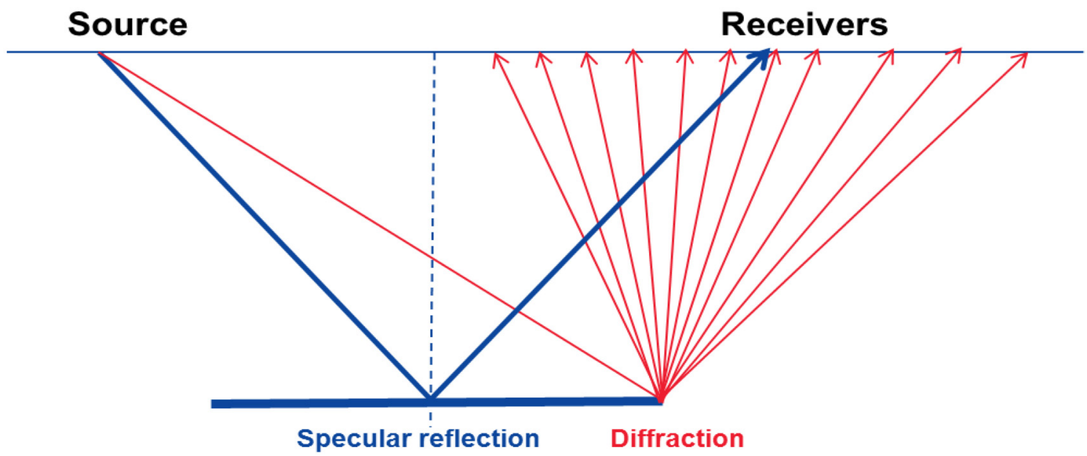

Figure 7—Schematic illustration of the primary specular reflection (the blue raypath) that follows the Snell's law, and the diffracted waves from an edge or corner (red raypaths) that do not follow the Snell's law.

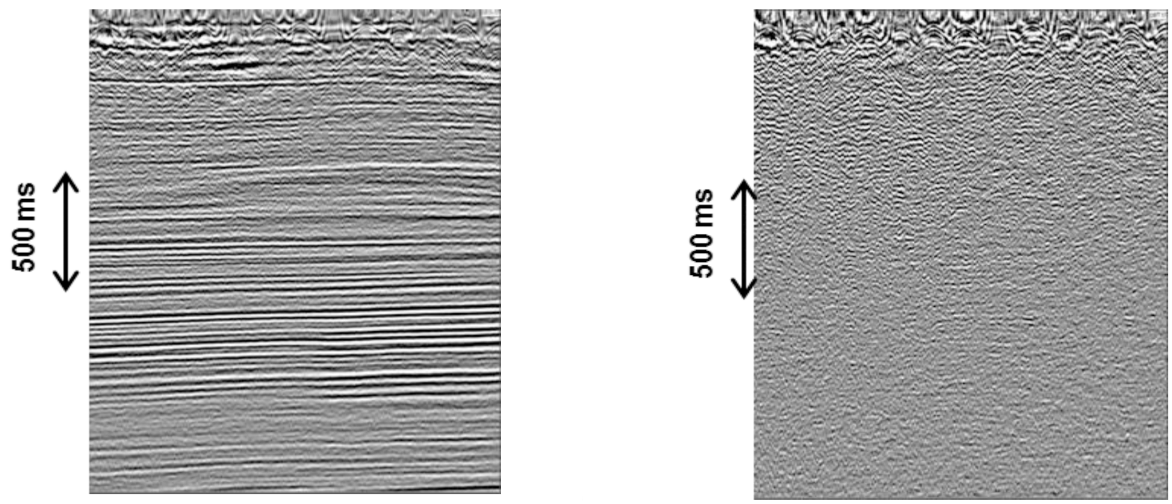

Figure 8—A cross section from the cross line showing primary reflections (left) and diffraction (right) separated from reflection on pre-migration stack. Note that noise and OBC footprint mask diffraction signals at this stage and a workflow was designed to suppress footprint and isolate/focus diffraction signals.

Figure 9 shows an example to compare diffraction imaging with conventional reflection imaging for the shallow areas where mud loss was encountered. We can see that the collapsed features as highlighted by red circles are more clearly imaging by the diffraction data than by the conventional reflection data. When we compare the seismic anisotropy and diffraction volumes, we find some compelling regions where there are similarities, and some features not mapped from previous data. Figures 10 to 12 compare the magnitude of seismic anisotropy with diffraction imaging (after color blending) and conventional reflection amplitude data for three different levels in the target 2 and 3 reservoirs. The regions have distinct lineations on the diffraction volumes, some at a finer scale than previously mapped for the geological model. Immediately south of the graben, there are regions of NE-tending lineations. These are in the same orientations of the dominant fracture orientation and correlate to a region of high anisotropy). Interestingly NE/SW lineaments lines up with main direction of fluid movement and Figure 11 is approximately in the target 3 level where we see most communication. One interesting thing is that most documented flow is north of the central graben but here we can extract most character south of it. There is also a correlation between WNW-trending lineations on diffraction, a region of high anisotropy, and a prominent mapped -trending fault near the southeast corner of the study region. In these cases, the high seismic anisotropy may represent fracture damage associated with the faults.

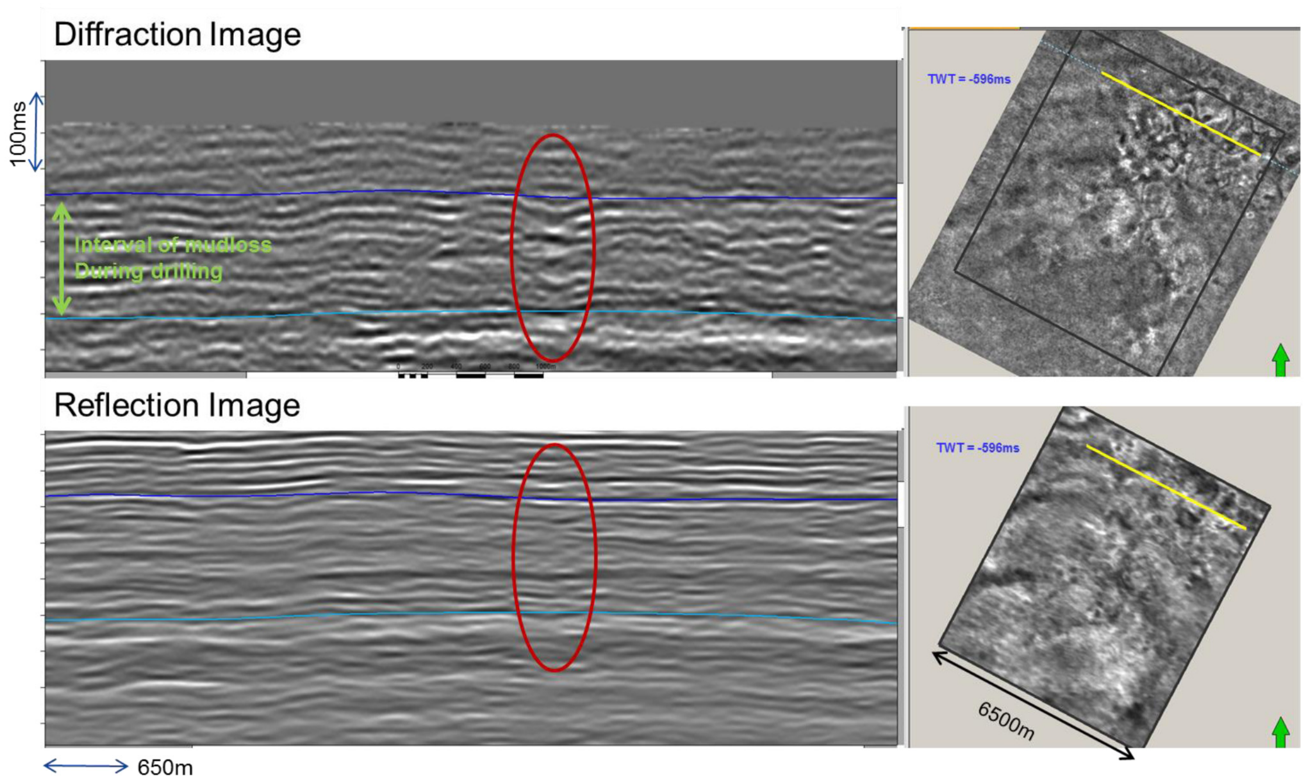

Figure 9—Comparison of diffraction imaging (upper) with conventional reflection imaging (lower) for the shallow areas where mud loss was encountered. We can see that the collapsed features as highlighted by red circles are more clearly imaging by the diffraction than by the conventional reflection.

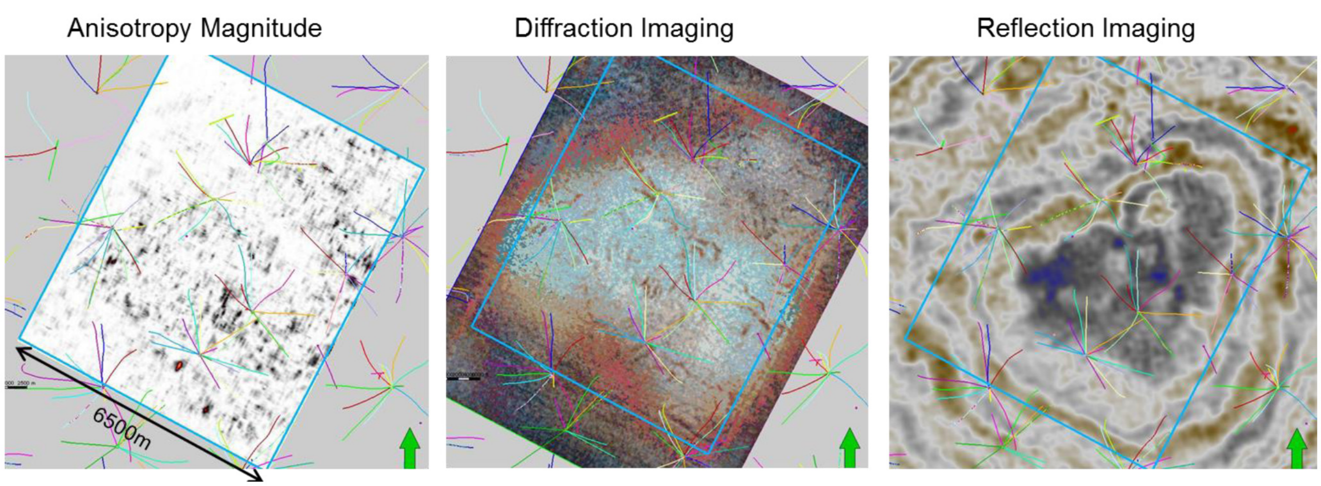

Figure 10—Comparison of anisotropy magnitude (left) diffraction imaging with color blending (middle) and the conventional reflection imaging at the Target 2 reservoir horizons. Notice the observation of interesting NE/SW character which lines up with main direction of fluid movement. One interesting thing is that most documented flow is north of the central graben but here we can extract most character south of it. Regions with high anisotropic magnitude which shows disperse characteristics correlate with anomalous areas in diffraction imaging.

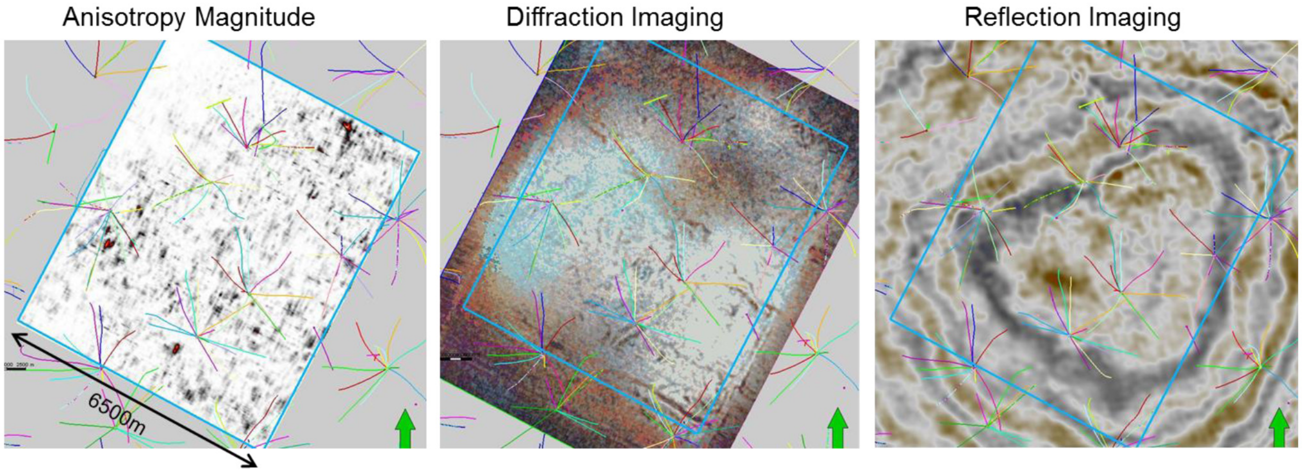

Figure 11—Same as Figure 10, but 12 ms deep in the reservoirs. Note the dispersed characteristics in anisotropy magnitude map and the high anisotropic area in the west correlate with anomalous features in diffraction imaging.

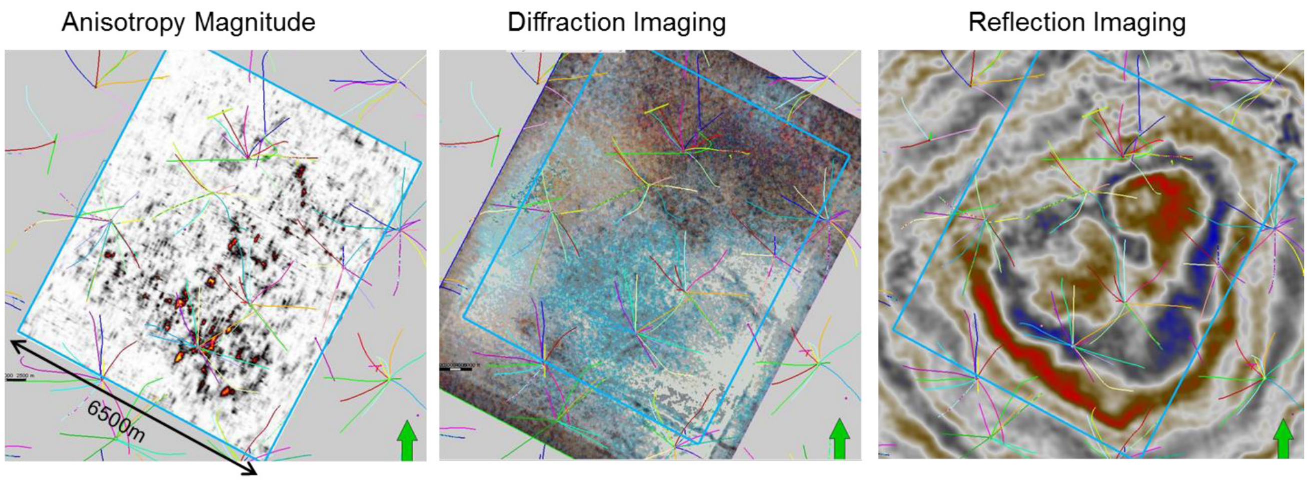

Figure 12—Same as Figure 10, but 36 ms deep in the reservoirs (near the base of target 3 reservoir). Note the areas with strong anisotropy magnitude correlate well with regions with anomalous features in diffraction imaing.

Modeling Study: Resolution, Detectability and Overburden Effects

Integration of different data faces challenges because of resolution, detectability and sensitivity issues. We perform synthetic modeling using the full wave anisotropic reflectivity method with the following objectives: (1) to determine uncertainties associated with seismic anisotropy to address sensitivity, detectability and resolution (i.e. applicability and limitations); (2) to understand overburden effects; (3) to investigate the azimuthal anisotropic response of fracture corridors and diffuse fractures. Figure 13 shows a comparison of seismic anisotropy magnitude (with marked horizons) with borehole fracture data (core and dipole sonic anisotropy). We can see that seismic derived "*fracture*'" attributes have much lower vertical resolution than borehole data, and therefore it is difficult to distinguish if fractures are confined to the top, middle or base of reservoirs from seismic data. While core data and dipole anisotropy suggest most fractures are confined to the top and lower parts of the reservoirs. For a stacked reservoir zones, seismic anisotropy at lower reservoirs can be influenced by the presence of fractures in upper layers. Thus, there is a need to understand the effects of overburdens. It is very likely that fractures seen in core samples are related to ‘diffuse’ fractures. The question is can we use seismic anisotropy to discriminate diffuse fractures and fracture corridors? In the following synthetic examples, fractures are represented as "*effective media*" (Liu and Martinez, 2012). By definition, scatterings or diffractions from individual fractures are not modeled.

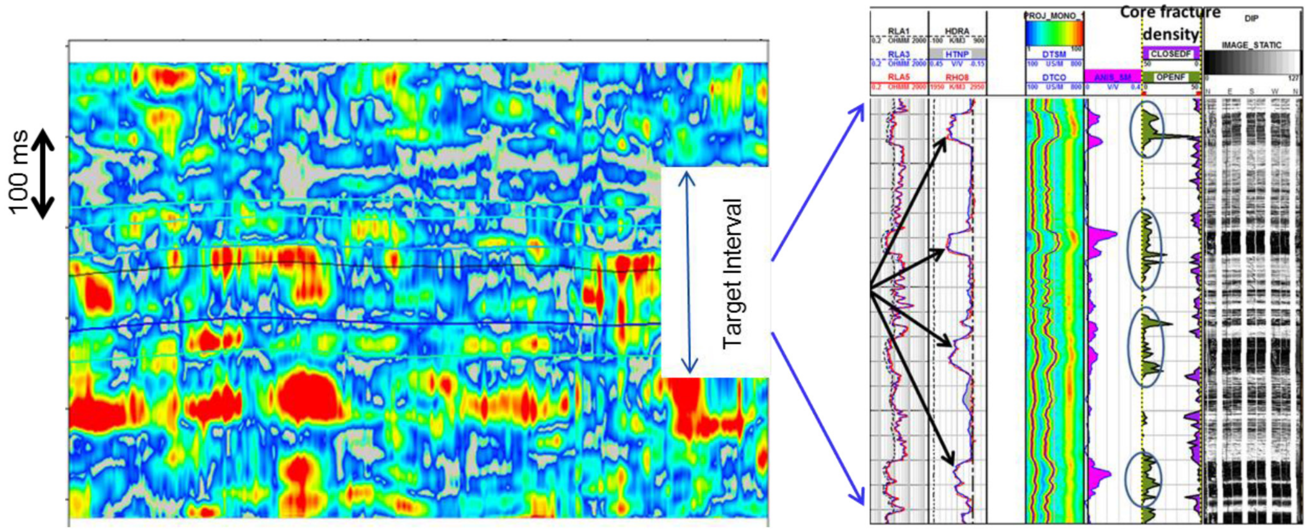

Figure 13—Seismic anisotropy magnitude as compared with borehole data (core and dipole anisotropy) indicating the challenge due to resolution and sampling issues.

Effects of the fracture zone position within a reservoir

We build a simple three-layer reservoir model with the fractured layer sandwiched between two half spaces (the parameters are given in Table 1). The source and receivers are located in the top half space and is 1000 m above the reservoir layer. We consider 4 models with fracture zone at top (model 1), middle (model 2), base (model 3) and both middle and base (model 4). We then pick the amplitudes from the top reflections (trough) and base reflections (peak) for each model and fit the azimuthal amplitude variations with a $\cos 2\phi$ function (Liu and Martinez, 2012). The magnitude of anisotropy is defined by *anisotropy%=(Max Amp-Min Amp)/Average Amp* $\times$ *100*. The results from all the four models are shown in Figure 14 and summarized in Table 2. We observe that the positions of fracture zones have an influence on both top and base azimuthal amplitude variations. As the reservoir thickness increases, the fracture on the lower part of the layer does not influence top azimuthal variations. The base reflections are much more strongly affected regardless of the positions of fracture zones, though they are less influenced if the fracture zones are confined to the center of the reservoir layer. The maximum and minimum anisotropy orientations are also dependent on the positions of fracture zones, which may be another reason for the 90° ambiguity in determining fracture orientation from seismic anisotropy.

Table 1—Model parameters

	Vp (m/s)	Vs (m/s)	Density (gcc)	Fracture density
Upper	5447	2969	2.596	0
Reservoir	3418	1992	2.230	0.12
Lower	5447	2969	2.596	0

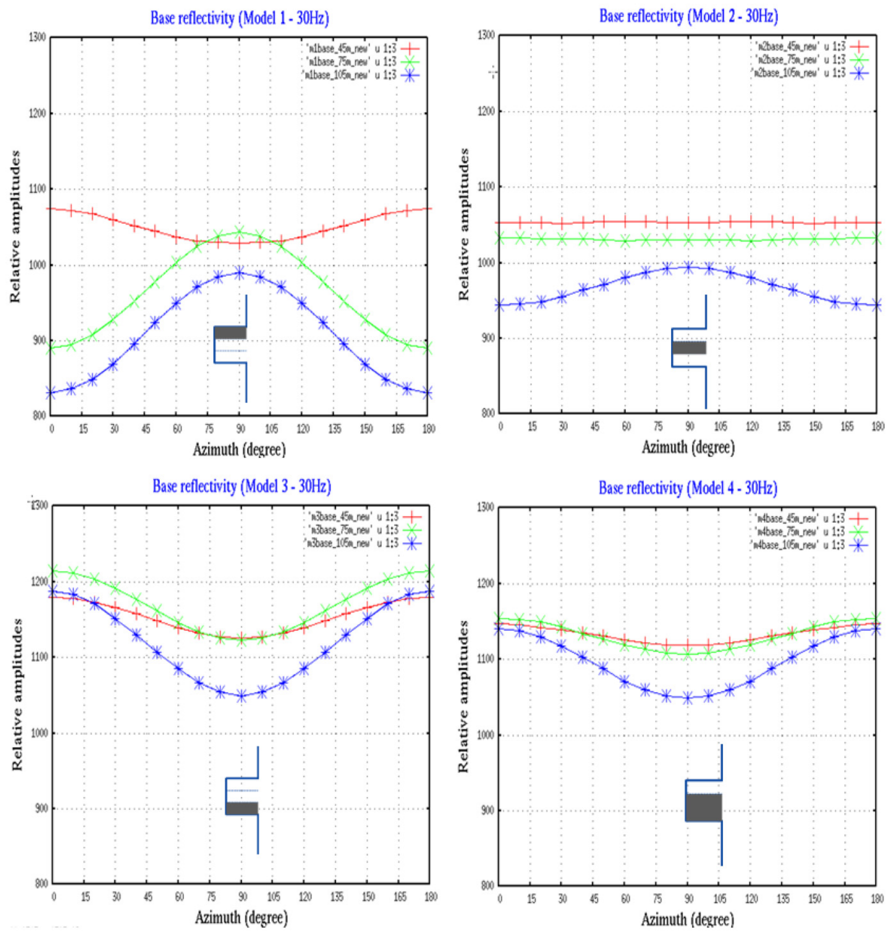

Figure 14—Azimuthal variations of base amplitudes computed from synthetic seismograms for three different thicknesses (red=45m, green=75m and blue=105m).

Table 2—Summary of estimated anisotropy from the modeled data for the offset of 3000, The model geometries and the position of fracture zones are illustrated on the left side

Model	Thickness (m)	Top (%)	Base (%)
1	45	8.1	4.2
	75	6.5	15.8
	105	6.2	17.4
2	45	2.4	0.3
	75	1.5	0.5
	105	0.06	5.2
3	45	0.4	4.6
	75	0.13	7.8
	105	1.2	12.3
4	45	2.7	2.5
	75	1.5	4.2
	105	0.04	8.3

Diffuse fractures vs fracture corridors

In the second set of models, we attempt to model the response of diffuse fracture vs fracture corridors. Several models have been considered with an attempt to investigate the effects of diffuse fractures and fracture corridors (simplified reservoir models for the study field). Models 1 to 3 are intended to represent fracture corridors (fractures cutting through different lithologies), while models 4 to 6 are for diffuse fractures (fractures are confined to individual layers). We have picked amplitudes for the offset of 3000m for the three major horizons: T1 base. T2 base and TA base, and plotted them as a function of azimuth. Figure 15a shows examples of modeled azimuthal variations from diffuse fracture model with fractures only in T1. We observe strong variations in amplitudes for all intervals (T1, T2 andT3). The variations in T2 and T3 are due to the fractures in the upper layer (T1), which is a clear demonstration of the overburden effects. For comparison, an example of long fractures across the entire interval (fracture corridor) is given in Figure 15b. As expected, we see azimuthal variations for all three key horizons. Comparing two models (Figures 15a and 15b), we find that both models give rise to strong azimuthal variations except the difference in polarity for T2 and T3 reflectors, i.e. the minimum and maximum in the reflected amplitudes. So we may conclude that it is difficult to distinguish between diffuse fractures and fracture corridors without careful analysis of the polarity and modeling study.

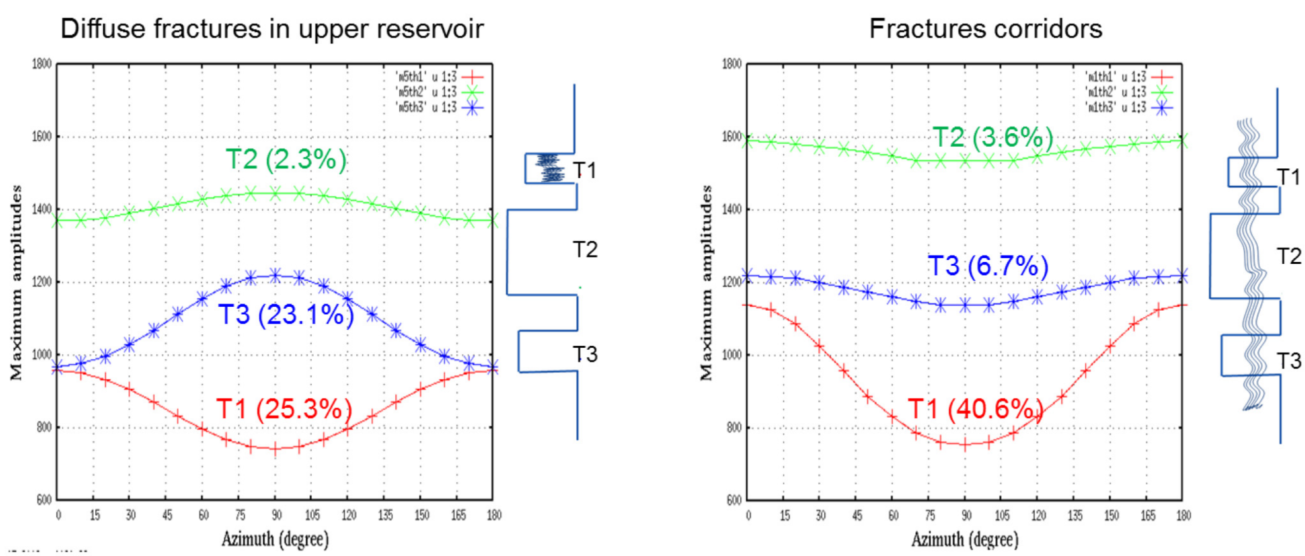

(a) (b)

Figure 15—Azimuthal variation of base amplitudes for three different intervals. Note that diffuse fractures (a) and fracture corridors (b) can cause similar azimuthal variations in magnitude, and there is a 90o change in anisotropy angles indicating 90o orientation ambiguity. This result indicates that it may be difficult to distinguish between diffuse fractures from fracture corridors from anisostropy magnitude magnitude alone. The numbers in bracket indicate the percentage of anisotropy computed by the difference of maximum and minimum amplitudes divided by the average value.

Overburden effects

Figure 16 shows the comparison of the azimuthal amplitude variations for two diffuse fractures in T1 (a) and in T3 (b). As expected, if fractures are in T3, we only see azimuthal variations the base of T3, and there is no azimuthal variations associated with the reflectivities in T1 and T2. In contrast, if fractures are only in T1, we can strong azimuthal variations in all the major horizons – strong evidence of overburden effects. This may explain the stacked anisotropy anomalies that are observed in Figure 6.

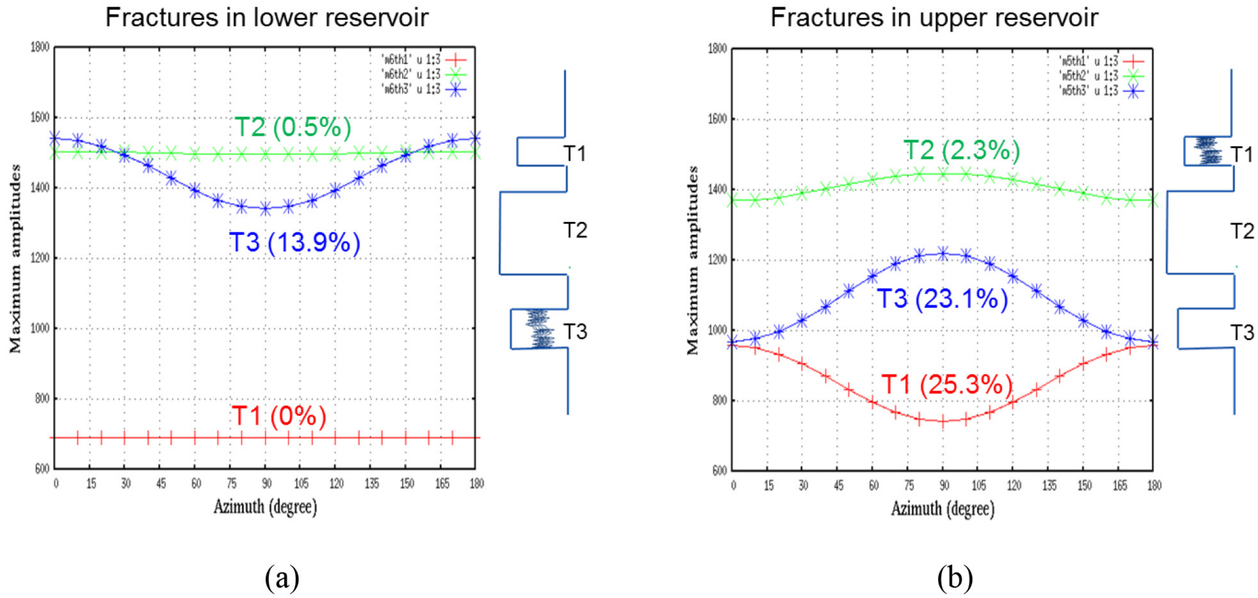

Figure 16—Azimuthal variation of base amplitudes for three different intervals. Overburden can have a significant effect on azimuthal variations, i.e. fractures in thin upper reservoirs can cause apparent azimuthal amplitude variations in the lower reservoirs (b). However, fractures in the lower reservoir do not cause azimuthal variations in the upper reservoir. The numbers in bracket indicate the percentage of anisotropy computed by the difference of maximum and minimum amplitudes divided by the average value.

Overburden effects have been noted by Liu et al. (2011); Ikawa and Mercado (2010); and Luo et al. (2007). Note that in a recent publication, Liu et al. (2015) have performed 3D synthetic study of estimating the fracture density of small-scale vertical fractures when large-scale vertical fractures are present. They use the synthetic data to investigate the ability to infer the properties of the small-scale fractures in the presence of the large-scale fracture set, and find that fracture density of the small-scale fractures can be reliably inferred even in the presence of large-scale fractures having significant compliance values. This is encouraging and implies that seismic anisotropy may help to provide information about small (diffuse) fractures, while diffraction imaging should help to resolve relatively large fractures.

The modeling studies presented here have highlighted the complexity of fractures on azimuthal anisotropy, and help to eliminate uncertainties in interpreting seismic anisotropy attributes:

- *Detectability and resolution*: For thin reservoirs (less than half the wavelength), it is difficult to discriminate fracture zone in the reservoirs. Fractures in the top, middle and lower part of the reservoirs will cause top and base reflectivity to be azimuthally anisotropic though their magnitudes can be different depending on where the fracture zones are. For thick reservoirs, there is strong sensitivity in reflections from top and base of the reservoirs to where the fracture zone is within the reservoir. Top reflectivity is insensitivity to fractures when they are in the middle or base of the reservoirs in contrast to thin reservoirs. Base reflectivity, however, is sensitivity to positions of fracture zones.
- *Overburden effects*: The overburdens have significant effects on the anisotropy. If we see anomalies along vertically in several intervals, we may say that the upper anomaly has to be removed before we interpret the lower anisotropy from fractures within that interval. However, if we see anomalies in lower intervals, but there is no anomaly in upper intervals, we can confidently say that the lower anomalies come from the local intervals.
- *Diffuse vs fracture corridors*: It is difficult to distinguish between fracture corridors and overburden diffuse fractures from anisotropy magnitude. However, overburden diffuse fractures seem to cause a 90° azimuth shift, while fracture corridors do not. Therefore combining the magnitude and

orientations, we may tell if the anomalies come from overburden diffuse fractures or fracture corridors. In any case, we suggest that synthetic modeling is necessary to add the interpretation.

Data Integration and Interpretation

Seismic anisotropy and core data

We compared the magnitude of anisotropy with the fracture intensity from core data, calculated over intervals defined by the seismic interpretation surfaces. Figure 17 compares the relative intensity of fractures with the magnitude of seismic anisotropy for the three reservoirs with core data. Overall in the south of the study area, the relative anisotropy magnitude is stronger than in the north. We also compared the azimuth of anisotropy with the orientation from core data with the azimuth extracted for the seismic interpretation surfaces (not shown here). The azimuth of seismic anisotropy represents the direction of greatest measured AzAVO, measured from geographic north. The azimuth of seismic anisotropy is poorly defined where the magnitude of anisotropy is small. Additionally, the calculation of the direction of the seismic anisotropy has an inherent 90° ambiguity, such that azimuth 45° could equally be azimuth 135°. Note that seismic anisotropy azimuth is potentially influenced by the acquisition orientations, which for this survey is N27°E (inline) and N117°E (crossline), and was addressed in the previous study (Liu et al., 2011). Note that the south area tends to have high fracture density where anisotropy magnitude is also large. For target reservoir T1, seismic anisotropy shows best alignment with fractures from Well A, Well B, and Well C. For target reservoir T2, seismic anisotropy shows best alignment with fractures from Well D and Well C. For target reservoir T3, seismic anisotropy shows best alignment with fractures from Well A and Well I.

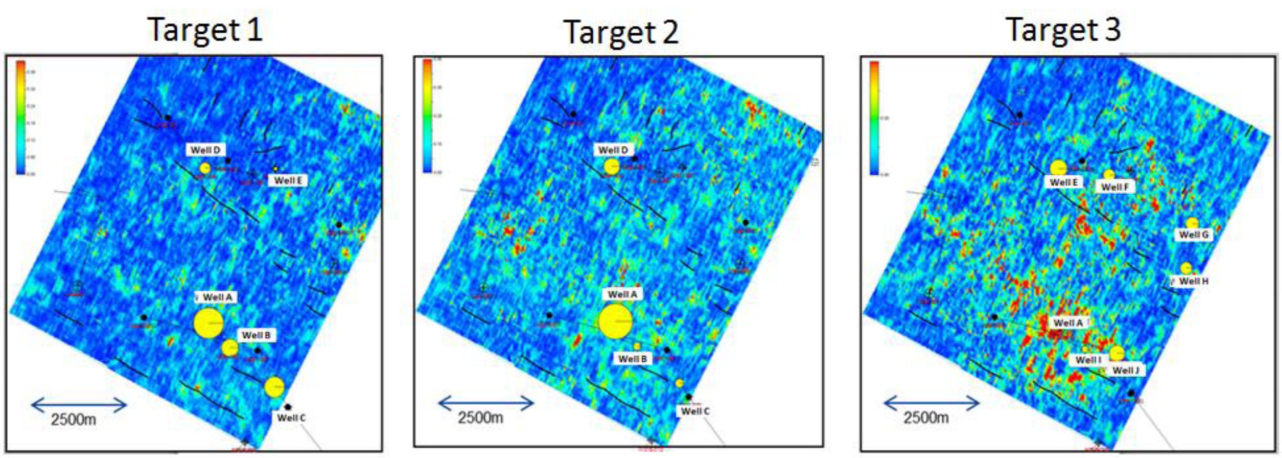

Figure 17—T2: Comparison of relative fracture intensity from core for open fractures and seismic anisotropy magnitude. Note that the south area tends to have high fracture density where anisotropy magnitude is also high.

Seismic anisotropy and dynamic data

In general, the region south of the central graben is a region of high seismic anisotropy on the maps for T1, T2, and T3. This trend is consistent with the region of the history match challenges (Figure 18). Production Logs (PLT) and pressure transient tests (PTA) potentially show evidence for flow from fractures and faults. Production logs (PLT's) in the study were screened to test whether zones of fluid influx correlated with the onset of a high anisotropy magnitude, with the assumption that fractures cause both high anisotropy and high fluid flux. For the available PLT's, we plot all the log curves against the magnitude of anisotropy volume. Where the logs show a high rate of change or ″kinks″, we interpret high fluid influx. In most cases, the cumulative water or cumulative oil curve commonly showed these features the best. In some cases the temperature log was a good indicator of fluid flux. Figure 19 show examples of likely PLT influx points near high anisotropy. Figure 20 show examples of PLT influx points that are likely stratigraphically controlled and do not directly correlate with the seismic anisotropy pattern.

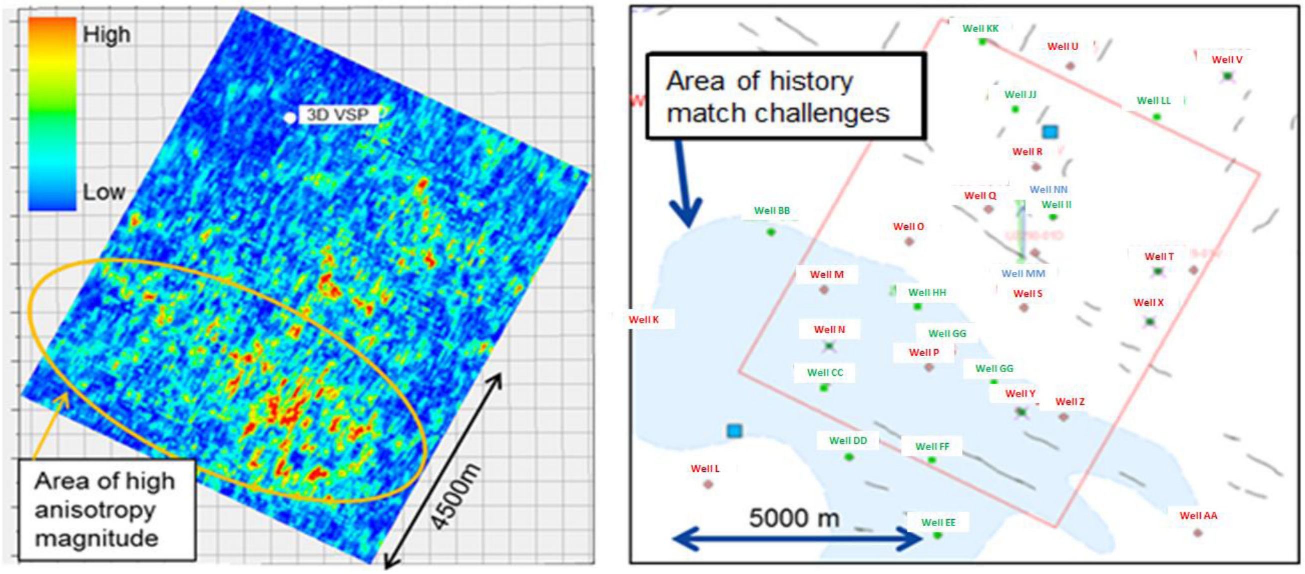

Figure 18—Comparison of extracted anisotropy magnitude at target 3 base (left) and the area of history match challenges. There is quatitative correlation between the areas of history match challenges with high seismic anisotropy magnitude.

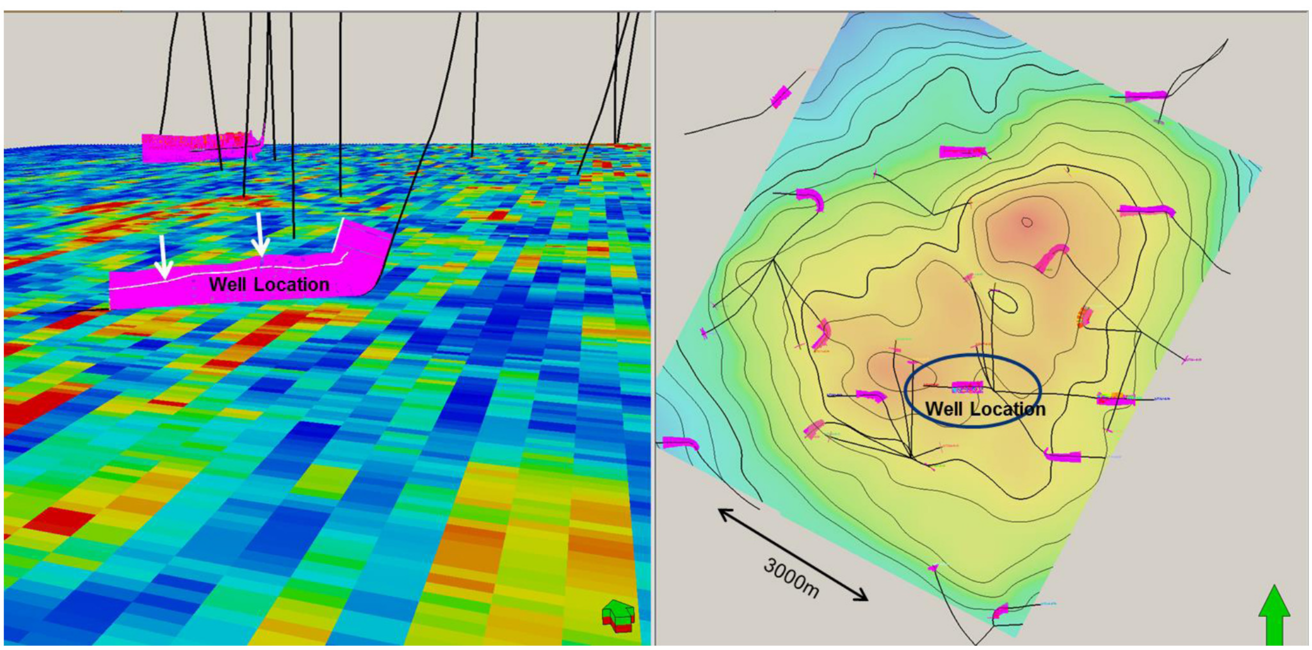

Figure 19—Comparison of seismic anisotropy with cumulative water log (Qwat) and cumulative oil log and the map location of study PLT's for the study area area and a horizon well location shown on the right. Qwat (pink) and Qoil (white) have kinks that maybe local influx, but good correlation with anisotropy magnitude

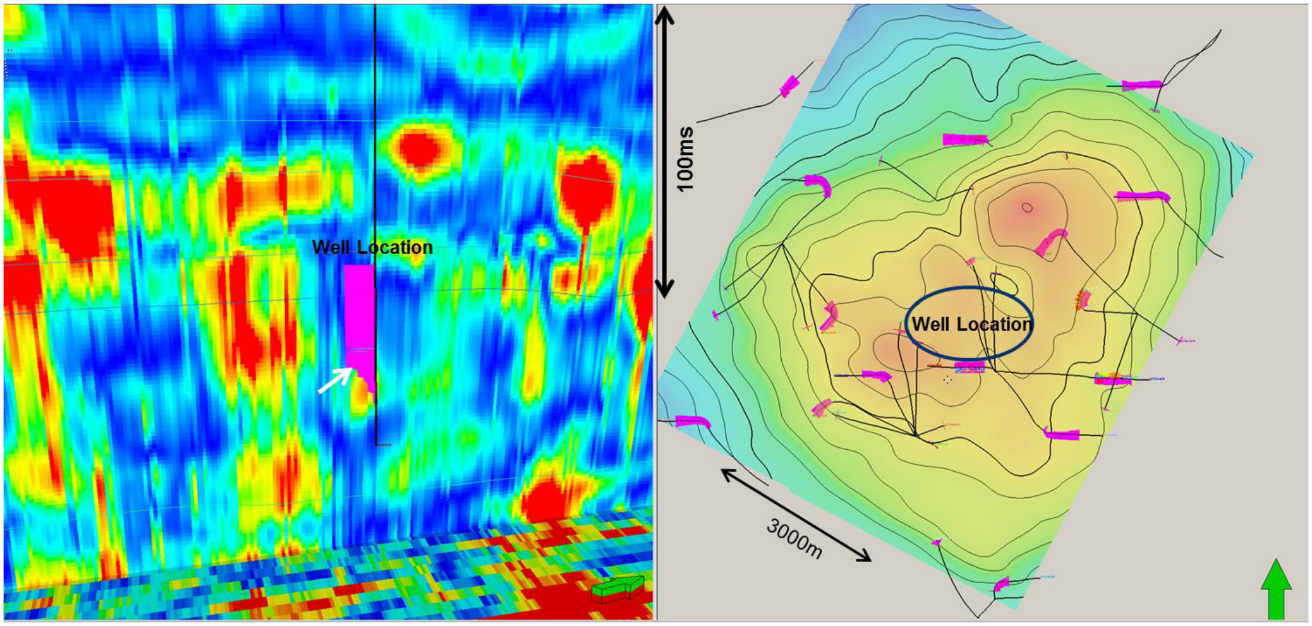

Figure 20—Comparison of seismic anisotropy with cumulative total fluid (Qtotal) and the map location of study PLT's for the study area area and a vertical well location shown on the right.

Diffraction data and mud loss in the shallow interval

The karst features in the diffraction data generally occur in zones where mud-loss has occurred during drilling, adding significant cost to the highly lateral wells. Figure 21 compares the diffraction imaging and reflection imaging at a shallow interval which corresponds to the stratigraphic zone where we encounter most losses. From the reflection data, we see chaotic characteristic which is unpredictive but the correlation of the diffraction with the losses in the northern half of the study area is very encouraging. The dynamic loss of fluid during drilling is potentially an indicator of karst zones. The mud-loss data comprise a point-set coded by the categories (1) no loss (2) partial loss, or (3) complete loss in the shallow intervals. There is a lack of complete loss in the southeast corner of the study region, where there are few features on the diffraction attribute (Figure 21). Complete losses are concentrated in regions that appear to relate to the dark zones on the diffraction, largely in the north and western part of the study region. Further validation work is needed to understand how predictive the diffraction data will be for well planning. A detailed comparison between diffraction imaged karst features with the fluid loss data is shown in Figure 22, where we compare those regions of loss with the shape of the features in the diffraction data. Blue is partial losses, green are complete and purple are no losses. The complete and partial spheres are positioned at the actual reported depth; the no losses wells are placed either at the top of the horizon of interest or at an average depth of the horizon of interest. Of course, there are lots of caveats on losses data and their positioning but due to the fact that almost all of the losses fall roughly in two stratigraphic levels gives us confidence there is a geological basis to their occurrence, not just drilling mud, mechanical issues, etc. The interesting karst-like features that we see in the data vertically encompass both of the stratigraphic levels and the zone in between.

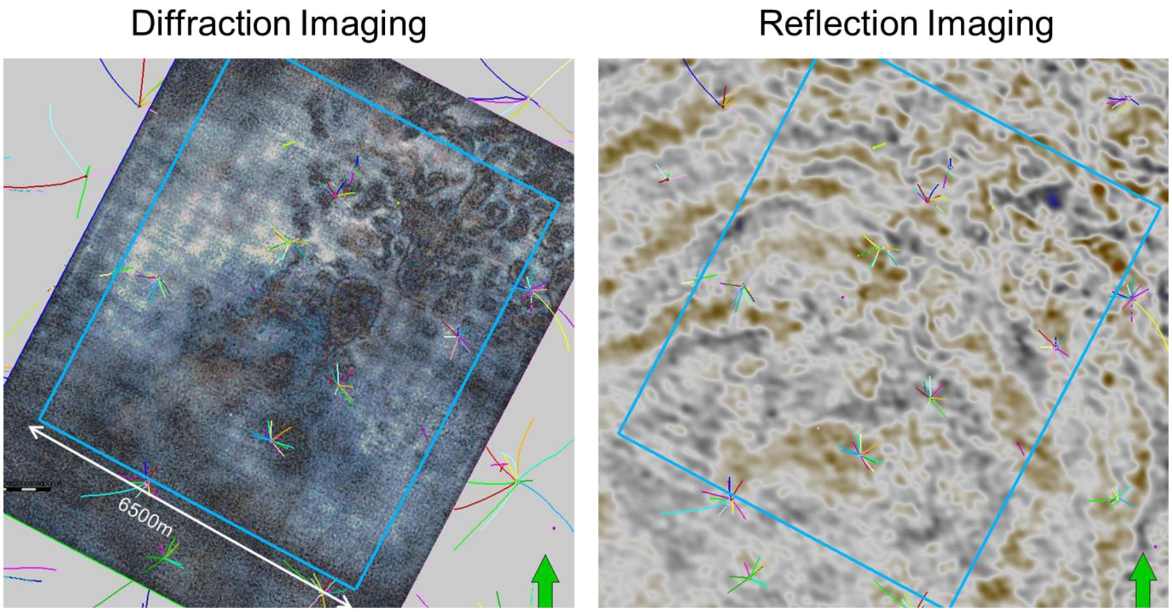

Figure 21—Comparison of diffraction images (left) and reflection imaging at the shallow interval which corresponds to the stratigraphic zone where we encounter most losses. The reflection data shows chaotic character which is unpredictive but the correlation of the diffraction with the losses in the northern half of the study area is very encouraging.

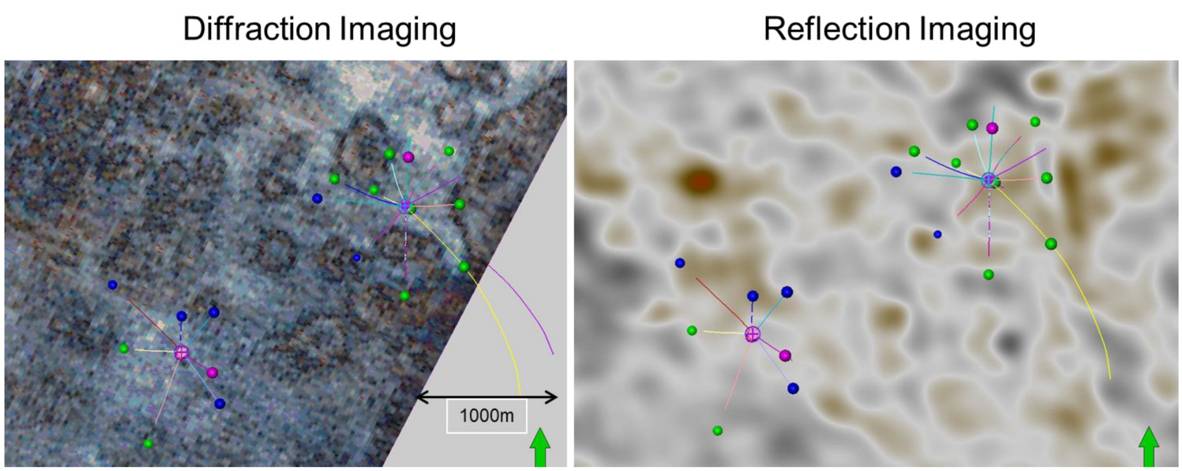

Figure 22—Comparison between diffraction imaged karst features with the fluid loss data. Blue is partial losses, green are complete and purple are no losses. The complete and partial spheres are positioned at the actual reported depth; the no losses wells are placed either at the top of the horizon of interest or at an average depth of the horizon of interest.

Summary

We have presented a case study of fracture characterization by integrating borehole data with a variety of seismic attributes in a carbonate reservoir. Seismic anisotropy complements other attributes. There is a qualitative correlation between the area of the history match challenges with the area strong magnitude of seismic anisotropy. In the interpretation of seismic anisotropy in terms of natural fractures, we have to consider the resolution and overburden issues. Seismic anisotropy appears to respond to diffuse fractures and can highlight regions of potential high fracture intensity area. However, we cannot discriminate diffuse fractures from fracture corridors with sufficient confidence. There are common features that can be identified in different attributes, and the differences do exists and may indicate different scales of fractures. It is important to choose the right stage in the seismic processing flow to preserve diffraction signals. Diffraction attributes as enhanced by color-blending have revealed more detailed geological features in overburden (e.g. karsts) and reservoirs (e.g. lineaments) than in reflection data and a comparison with mud loss data in the shallow zones looks promising and shows a good correlation between mud loss and collapsed features. This work has demonstrated the applicability of the using various seismic attributes for fracture characterizations and it also highlights the need to integrate different attributes together with well data in order to increase confidence in fracture interpretation.

Acknowledgements

We thank the support of ADNOC, JODCO, EMAD and ZADCO and for permission to present the results of this work. We thank Math Williams and Ewart Edwards for discussion and for providing information about fracture information of the study area. Z-Terra performed the diffraction imaging.

References

Burnett, W.A., Klokov, A., Fomel, S., Bansal, R., Liu, E. and Jenkinson, T. [2015] 3D Seismic diffraction interpretation at Piceance Creek. *Interpretation,* **3,** SG1-SF14.

El-Awawdeh, R., Khouri, N., Neyadi, A., Shevchek, Z., Shebl, H., Edwards, H.E., Gombos, A. and Johns, M. [2008] *3D seismic evidence of tertiary — Cretaceous karsts and collapse disturbance from offshore oilfield in Abu Dhabi and outcrop analogs from Jebel Hafit, UAE*. SPE-118006.

Edwards, E., Sit, H., Bu Al-rougha, H., Sultan, A. and Khouri, N. [2006] *Tectonic history and basement fault control on structural development of an offshore field,* Abu Dhabi. SPE-101416.

Ikawa, H. and Mercado, G. [2010] *A case study of seismic anisotropy analysis on multi-azimuth OBC seismic data in an offshore carbonate oil field, UAE*. SPE-137986.

Liu, E. and Martinez, A. [2012] *Seismic Fracture Characterization: Concepts and Practical Application*. EAGE Publication.

Liu, E., Zelewski, G., Lu, C.-P., Reilly, J.M. and Shevchek, Z.J. [2011] Mitigation of overburden effects in fracture prediction using azimuthal AVO analysis: an example from a Middle East carbonate field. *The Leading Edge,* **30,**750–756.

Liu, Y., Dong, N., Fehler, M., Fang, X. and Liu, X. [2015] Estimating the fracture density of small-scale vertical fractures when large-scale vertical fractures are present. *J. Geophys. & Eng*., **12,** 311–320.

Luo, M., Takahashi, I., Takanashi, M. and Tamura, Y. [2005] Improved fracture network mapping through reducing overburden effect. *The Leading Edge,* **24,** 1094–1098

Guilloux, Y., Tarrass, I. and Boelle, J.L., Landa, E., Buzlukov, Lafram, A. and Radigon, M. [2012] *Wide azimuth seismic processing for UAE carbonate reservoir characterization*. SPE-162324.

Sturzu, I., Popovici, A.M., Moser, T.J. and Sudhakar, S. [2015] Diffraction imaging in fractured carbonates and unconventional shales. *Interpretation,* **3,** SF69-SF75.

Sultan, A., Zhang, J., Edward, H.E., Hage, A., Shahata, K. and Jan, K. [2011] Role of high quality seismic in field development and production through case studies from a giant offshore carbonate field, Abu Dhabi. UAE. *Expanded SEG Abstract,* **30,** 1103–1107.

Reilly, J.M., Shatilo, A.P. and Shevchek, Z.J. [2010] The case for separate sensor processing: Meeting the imaging challenges in a producing carbonate field in the Middle East. *The Leading Edge,* **29,** 1240–1249.

Sturzu, I., Popovici, M., Moser, T.J. and Sudhakar, S. [2015] Diffraction imaging in fractured carbonates and unconventional resources. *Interpretation,* **3,** SF69-SF79.

Zhang, J., El-Awawdeh, R., Shevchek, Z.J., Khouri, N., Sultan, A., Harris, C.E. and Reilly, J.M., [2010] Seismic-constrained reservoir property prediction—Example from a giant carbonate field offshore Abu Dhabi, UAE. *SEG Expanded Abstract,* **29,** 1312–1316.